
**OPTICS OF CLUSTERS,
AEROSOLS, AND HYDROSOLES**

Generation of Aerosol and Droplets in Binary Mixtures of Saturated Water Vapor with Air and Molecular Gases

**A. V. Klimkin^a, A. N. Kuryak^a, Yu. N. Ponomarev^a, A. S. Kozlov^b, S. B. Malyshkin^b, A. K. Petrov^b,
A. L. Kupershtokh^{c, d}, D. I. Karpov^{c, d}, and D. A. Medvedev^{c, d}**

^a*V.E. Zuev Institute of Atmospheric Optics, Siberian Branch, Russian Academy of Sciences,
pl. Akademika Zueva 1, Tomsk, 634055 Russia*

^b*Voevodsky Institute of Chemical Kinetics and Combustion, Siberian Branch, Russian Academy of Science,
ul. Institutskaya 3, Novosibirsk, 630090 Russia*

^c*Lavrentyev Institute of Hydrodynamics, Siberian Branch, Russian Academy of Sciences,
pr. Lavrentyeva 15, Novosibirsk, 630090 Russia*

^d*National Research Novosibirsk State University, ul. Pirogova 2, Novosibirsk, 630090 Russia*

*e-mail: tosha@asd.iao.ru, alex@asd.iao.ru, yupon@iao.ru, kozlov@kinetics.nsc.ru, msb@ngs.ru, petrov@kinetics.nsc.ru,
skn@hydro.nsc.ru, karpov@hydro.nsc.ru, dmedv@hydro.nsc.ru*

Received November 13, 2015

Abstract—Results of observation of the generation of aerosol particles and droplets in mixtures of saturated water vapor with air and molecular gases are described. The kinetics of generation of aerosol and droplets was studied in the absence of a monokinetic electron beam and under its influence on a gas mixed with super-saturated water vapor formed in the process of a controllable pressure discharge from a spherical chamber of 1.4 m diameter with the gas mixture into a vacuum reservoir ~ 40 m³ in volume. The generation kinetics was recorded by the low-angle laser beam scattering method (for droplets) and with an aerosol spectrometer (for particles). Experimental results show a significant dependence of droplet and particle generation on the ionizing radiation effect. The 3D computer simulation of the process of super-saturated water vapor condensation on ions by the lattice Boltzmann method (LBM) and molecular dynamics (MD) describes qualitatively the experimental results.

Keywords: atmosphere, clouds, molecules, aerosol, drop, phase transition, ionizing radiation, computer modeling

DOI: 10.1134/S102485601602007X

INTRODUCTION

Clouds in the atmosphere significantly influence the energy exchange between the Sun, atmosphere, and the Earth's surface. The cloud formation dynamics is controlled by processes of growth and evaporation of water drops. A major role of ionizing radiation in the cosmic nature of cloud formation and thunderstorm activity was established, for example, in [1–4].

Experimental investigations of water vapor condensation began more than 100 years ago by Wilson [5]. The dynamics of the water vapor condensation (actual for realizing cloud formation) in dependence on the type and the number of condensation centers, temperature variations, gas-vapor mixture pressure, and the presence of ionizing radiation was studied, as a rule, with the use of Wilson chambers of a small volume [4, 6].

In 2010, at V.E. Zuev Institute of Atmospheric Optics, Siberian Branch, Russian Academy of Sciences, the first version of experimental setup was designed for study of processes of saturated water vapor

nucleation in atmospheric air, which operated by the scheme of the Wilson chamber of the second type with a significantly larger volume of working chambers [7]. This setup allowed experiments on the dynamics of generation of aerosol particles and drops in a mixture of saturated water vapor with air of different degree of purification under adiabatic variation in the mixture pressure and electron beam exposure [8, 9]. Some results obtained (for example, the nature of the third maximum in the diagram of time dependence of the drop concentration [8]) were not uniquely interpreted because of their qualitative character.

In this paper, we describe experimental results on recording aerosol droplet formations in a mixture of saturated water vapor with air and binary mixtures with molecular gases obtained with an improved experimental complex [7], as well as the results of 3D computer simulation by the lattice Boltzmann equations (LBE) and molecular dynamics (MD) methods of super-saturated water vapor condensation on ions.

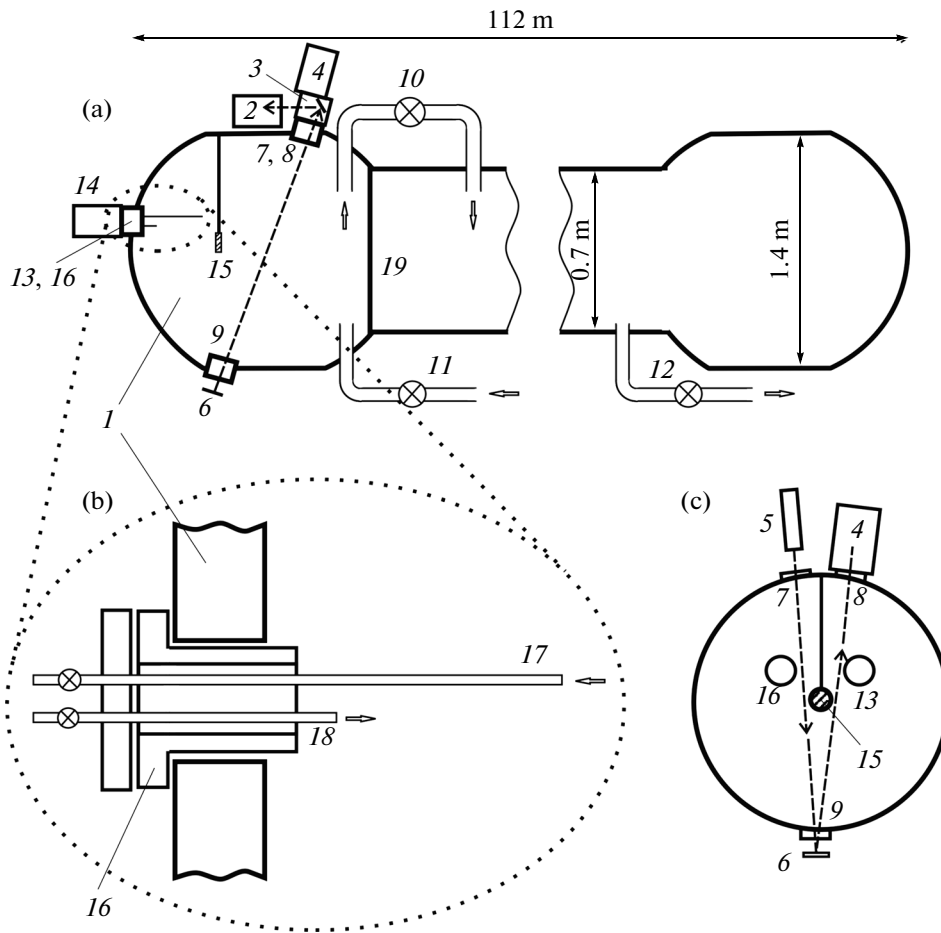


Fig. 1. Layout of the experimental setup: (a) general layout of the setup; (b) flange for connecting the photoelectric spectrometer of aerosol; (c) cell end: cell (1), photodetectors (2 and 4), block with rotary mirror (3), laser (5), mirror (6), flanges with windows (7, 8, and 9), vacuum valves (10, 11, and 12), flange for mounting the source of electrons (13), electron source (14), electrode (15), flange for connecting the photoelectric spectrometer of aerosol (16), tube for air sampling (17), tube for air discharge (18), and barrier (19).

INSTRUMENTATION

The instrumentation complex (Fig. 1) is intended for the study of processes of water vapor condensation and generation of water aerosol in different gases and gas mixtures with a pressure decrease and under the impact of a charged-particle beam. It is designed on the basis of a KA-1 optical cell made from a stainless tube with an inner diameter of 0.7 m and a length of 112 m. The cell ends are increased in size and have the form of cylindrical chambers. The diameter of the chambers is 1.4 m, the length is about 1.5 m. The total volume of the cell is 45 m³. The cell is divided by barrier (19) into two chambers: small one with a diameter of 1.4 m and volume of 1.5 m³ and a large one 43.5 m³ in volume. The small (exposure) chamber is intended for preparing mixtures of air and molecular gases with saturated water vapor, and the large chamber serves as a buffer volume, where a controlled release of the gas mixture from the exposure chamber proceeds. The chambers are connected with each other through air

valve (10) with a controllable vent rate (MKS Instruments, United States). In the system, as in a Wilson chamber of the second type, the water vapor saturation is produced through the pressure unloading from the small chamber to the large one.

Air is exhausted from both chambers to a pressure of 10⁻² Torr at open vacuum valve (10) through valve (12). Then, valve (10) is closed and air or a mixture of water vapor with molecular gas inflow through a system of filters and valve (11) to the small chamber until the pressure is 500 Torr. The humidity in the small chamber attains 100%. After that, a controlled pressure release is performed from the exposure chamber to the buffer, accompanied by the generation of particles and droplets inside the exposure chamber.

A small-size electron accelerator [10] is used as an electrons sources (ES) (14). It emits an electron beam with an energy of no lower than 80 keV and a length at half maximum of 15 ns. The beam diameter at the ES output does not exceed 0.014 m. The beam

divergence is 48 degrees at an air pressure of 760 Torr and 15 degrees at a pressure of 250 Torr.

The appearance of big aerosol particles and drops in the exposure chamber was controlled by variations in the absorption and scattering of radiation of a single-mode single-frequency JDSU-1507-2 He–Ne laser (United States). Laser (5) radiation passed through the exposure chamber and returned to photodetector (4) from mirror (6). Photodetector (2) was used for the control of the laser output power. As photodetectors, photoelectric multipliers (PEM-79) were used.

A Scanning Mobility Particle Sizer 5.403 (SMPS) aerosol spectrometer (Grimm Aerosol Technik, Germany) is used to measure the particle size spectrum from 10 to 1100 nm; it is connected through flange (16). The experimental complex includes a vapor generator Lelit-PS09N (Italy), humidity and temperature sensor E + E Elektronic-E33-MFTI (Austria), and vacuum gauge Vacuubrand DVR5 (Germany). All windows in the body of the exposure chamber have controlled heating.

In order to control all sensors of the experimental complex, a specialized software package was developed based on LabView. The complex specifications are given below.

Overall dimensions, m	112 × 0.7
Overall dimensions of the chamber with ES, m	1.6 × 1.4
Vacuum of working chamber, Torr	10 ⁻⁵
Vacuum of buffer capacity, Torr	10 ⁻²
Energy of ES electron beam, no less than, keV	80
Divergence of electron beam, deg	
at a pressure of 1 atm	45
at a pressure of 0.3 atm	15
ES output electron beam diameter, m	0.014
Frequency of photodetector readings, Hz	1–10 ³
Relative error of photodetector signal measurements, %	0.5
Degree of purification of input air, no less than, %	99.9
Radiation wavelength, μm	0.63
Pressure sensor	Vacuubrand DVR5

Techniques for vapor-gas mixture preparation are described in detail in [8, 9].

EXPERIMENTAL RESULTS

The experimental generation of a liquid-droplet aerosol with a dependence on the rate of pressure discharge in a mixture of water vapor with air in the absence or presence of electron beam exposure is described in [8, 9]. It was shown in [8] that with a suf-

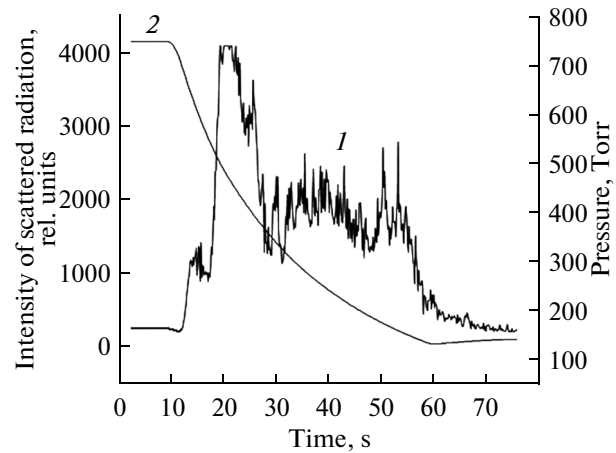


Fig. 2. Intensity of scattered radiation (*I*) and pressure drop (2) in the exposure chamber at a rate of pressure discharge of 30 Torr/s.

ficiently rapid pressure discharge that provides adiabatic widening of the vapor-gas mixture in the chamber, three peaks appear in the scattered laser radiation intensity signal (Fig. 2).

The first peak appears at 20 s and corresponds to the generation of water droplets on dust particles [7]. The second peak appears at 40 s as the pressure drops by 0.72–0.74 as compared to the initial mixture pressure. In this case, water vapor super-saturation is 3.9–4.50 and corresponds to the super-saturation under which the condensation of water vapor on ions is observed [11]. The nature of the third peak at 50 s in [7] is not ascertained definitely. It is also noted that an increase in the pressure discharge rate leads to an increase in the second peak intensity.

In [7], the formation of particles sized from 10 to 100 nm was studied together with the generation of droplets in the same experimental setup. A SMPS 5.403 aerosol spectrometer consisting of a selective column, where the particle sizing takes place, and a recording block, was connected to the exposure chamber (to flange (16), see Fig. 1). An aerosol-gas mixture was sampled from the chamber to the spectrometer through tube (17), and through tube (18) it returned to the chamber through the aerosol filter.

It is shown in [9] that generation of new particles was always recorded at the pressure discharge from a level of 500 Torr (Fig. 3). The authors supposed those particles to be condensation centers that remain from droplets generated inside the exposure chamber and partly dried up during their passage through tube (17) to the aerosol spectrometer. The estimates show that up to 10⁴–10⁵ 80-μm droplets per 1 L of a vapor-gas mixture appear in the exposure chamber at the pressure discharge.

When studying the pulse impact of an electron beam on a mixture of air with water vapor, it was established that the intensity of radiation scattered by drop-

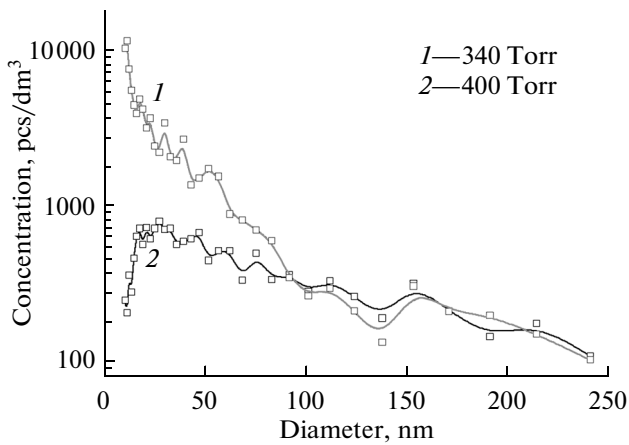


Fig. 3. Size distribution of aerosol particles forming as the pressure decreases.

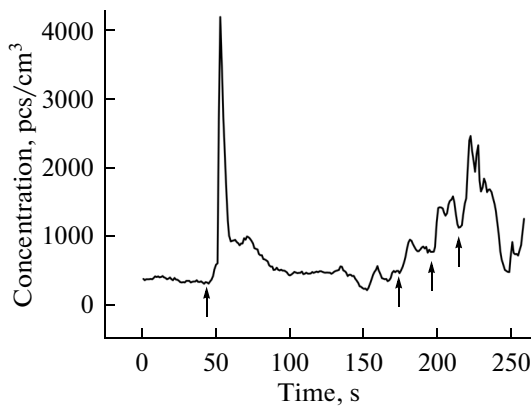


Fig. 4. Time dependence of the total concentration of particles with sizes higher 10 nm (arrows show the instants of the electron beam impact).

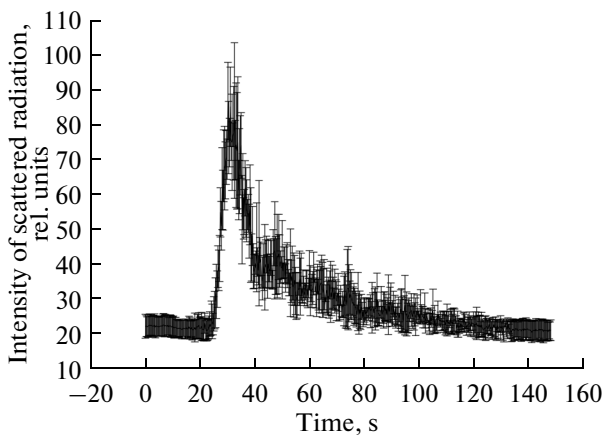


Fig. 5. Kinetics of the scattering radiation intensity (averaged over 6 points).

lets which are condensed on dust micro-particles (the first peak in Fig. 2) increases insignificantly. The intensity of scattering by droplets condensed on ions increases more than by an order of magnitude in this case. Figure 4 shows that the impact of an electron pulse in the volume of the exposure chamber (the air–water mixture pressure is 370 Torr and relative humidity is 100%) results in generation of many new particles ($\sim 4000 \text{ cm}^{-3}$). When the electron beam is turned on again, the concentration maxima of particles generated decrease. This can be caused by a decrease in the mixture humidity and precipitation of droplets on the chamber walls. Aerosol formation in model mixtures of saturated water vapor with CO_2 and nitrogen was studied with more accurate control of the pressure discharge rate and start. To do this, a pressure discharge valve (MKS Instruments, United States, type 253B) in the form of butterfly-shaped shutter with an inner diameter of 32 mm was installed. Together with the pressure sensor, the valve allows the computer-controllable flow of the gas mixture from the exposure chamber to the buffer. Its use made the repetitiveness of results no worse than 90% in a series of 6–10 sequential discharges at similar initial parameters of the gas mixture in the exposure chamber (Fig. 5).

Figure 6 does not show the formation of the drop fraction (light-scattering intensity) in binary $\text{CO}_2\text{--H}_2\text{O}$ (Fig. 6a) and $\text{N}_2\text{--H}_2\text{O}$ (Fig. 6b) mixtures.

MD SIMULATION OF THE INITIAL STAGE OF NUCLEATION

As is known, the critical size of a drop nucleus in vapor sharply increases when saturation decreases [12]. The appearance of ions in the vapor results in a decrease in the critical nucleus size. Continuous-field analogue and thermodynamic techniques allow simulation of the condensation process in the cases where there are nuclei of submicron sizes in the system, on which droplets can be generated. The process of nucleation on ions, where molecules settled down on an ion number in units or tens, is not considered. Therefore, in order to describe the initial stage of the nucleation, the MD method was used. Two models were actualized: ion in the saturated vapor of polar molecules and ion in the saturated vapor of nonpolar molecules with predetermined polarizability.

The spherical model of a molecule was used. Intermolecular forces were presented by two types of potentials. Symmetrical attraction and repulsion were described by the Lennard-Jones potential. The electric interaction between polar molecules and molecules and ions were described in the approximation of the point dipole put at the center of a molecule.

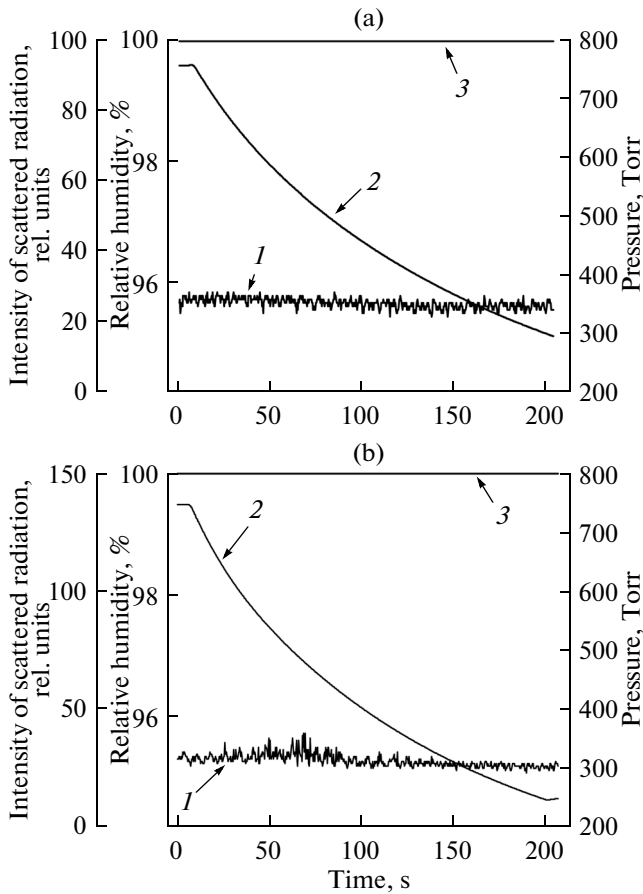


Fig. 6. Time dependence of scattered radiation intensity in (a) CO₂-H₂O and (b) N₂-H₂O mixtures at the pressure discharge inside the exposure chamber: scattered radiation intensity (1), pressure drop in the chamber (2), and relative humidity (3).

The interaction force between a pair of dipoles was calculated by the formula

$$F_{DD} = \frac{3}{r^5}((\mu_1 \cdot \mu_2)\mathbf{r} + \mu_1(\mu_2 \cdot \mathbf{r}) + \mu_2(\mu_1 \cdot \mathbf{r})) - 15 \frac{(\mu_1 \cdot \mathbf{r})(\mu_2 \cdot \mathbf{r}) \cdot \mathbf{r}}{r^7},$$

where μ_1 and μ_2 are the dipole moments of the molecules; \mathbf{r} is the radius-vector, and r is the distance between dipole centers. Forces acting between the dipole μ and ion were calculated by the formula

$$F_{ID} = Q \left(\frac{3(\mu \cdot \mathbf{r})\mathbf{r}}{r^5} - \frac{\mu}{r^3} \right),$$

where Q is the ion charge.

For polar molecules, the ion influence is reduced to their turn under the action of the ion field and drift to the range of strong field. In calculation of 3D rotations, an algorithm with application of quaternion algebra was used.

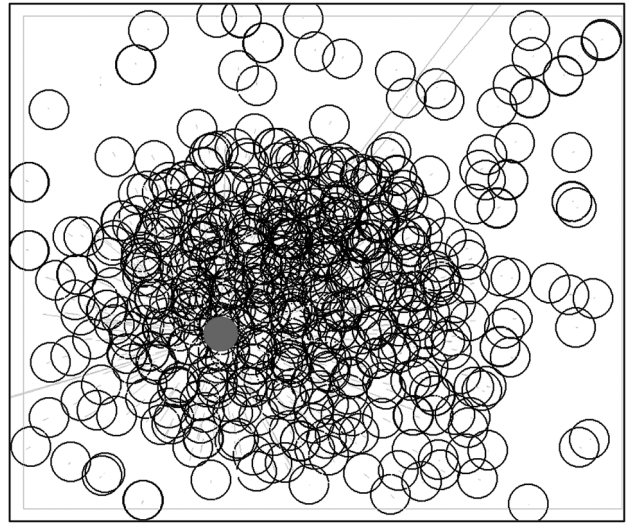


Fig. 7. Droplet around an ion (gray circle) located in the saturated vapor of neutral molecules polarized under the impact of electric field of the ion. Plane projection of the 3D-distribution of molecules.

In model calculations, which take into account the polarization of molecules by the ion field, an algorithm was used which allowed us to calculate the influence of fields of neighboring dipole molecules on the dipole moment. When computing the self-consistent field at the point of molecule location, the fields of an introduced ion and all molecules of the ensemble were taken into account. At each step of the MD calculation, values of dipole moments of molecules and of the local electric field were corrected using the iteration procedure [13], in accordance with new arrangement of molecules of the ensemble and the ion. Due to polarization in the ion field, molecules were attracted to the ion.

The attraction force of a polarized molecule to the ion is equal to $\sim r^{-6}$, while the force of the molecular attraction is $\sim r^{-7}$; therefore, the condensation on the ion proceeds faster than the density fluctuations in the vapor. At large droplet radii, the field strength decreases significantly more slowly than near the ion, and the growth is mostly determined by intermolecular interaction forces described by the Lennard-Jones potential. Figure 7 shows the nucleation in the gas of nonpolar molecules with constant polarizability.

In an inhomogeneous field, dipole molecules settle on an ion. The influence of the electric field on the dynamics of microdroplet generation is significant as long as the thickness of the dipole layer is equal to 2–3 diameters of the molecule. Thus, the simulation shows that the part of an ion reduces to formation of the layer of polarized molecules with a thickness of ~ 3 diameters of the molecule (droplet nucleus) around the ion.

The dynamics of nucleation on ions is studied at different values of vapor density. In order to record the

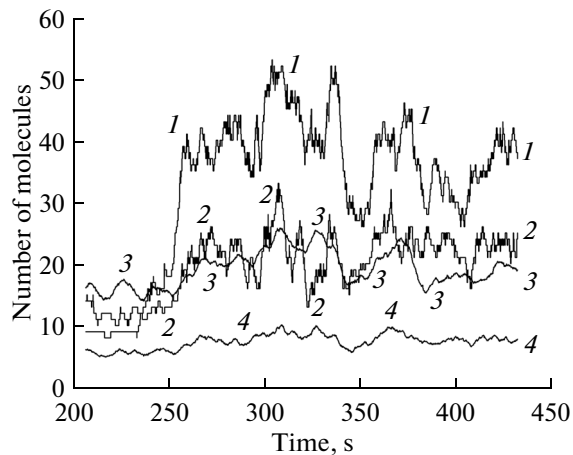


Fig. 8. Number of neighboring molecules in coordination spheres with the radii $R = 2$ (curves 2 and 4) and $R = 4$ (curves 1 and 3) of molecule diameters as a function of time for ion (curves 1 and 2) and vapor molecule (curves 3 and 4).

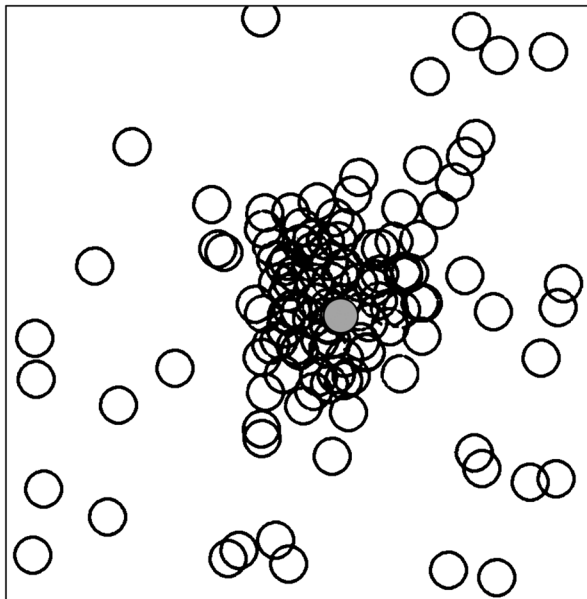


Fig. 9. Nucleus on an ion (gray circle) in vapor of polar molecules. Plane projection of the 3D distribution of molecules.

dynamics of nucleation on an ion, the number of molecules inside coordination spheres centered at the ion was calculated at equal intervals. Sphere radii were equal to two and four diameters of the molecule. To decrease the influence of fluctuations of the number of molecules in a coordination sphere on the result, the averaging over time intervals, approximately corresponding to 10000 steps in time of MD calculations, was carried out. Figure 8 shows the time dependence of the size of droplets generated on ions. For comparison, similar plots are presented for coordination spheres built around one of the vapor molecules.

The generation of micro-droplets on ion in the dense gas of polar molecules is calculated at different values of the vapor density. The calculations show that the influence of ion results in liquid phase nucleation on the ion (Fig. 9).

In an inhomogeneous field, dipole molecules settle on an ion. The influence of the electric field on the dynamics of microdroplet generation is significant as long as the dipole layer thickness is equal to 2–3 diameters of the molecule. At larger droplet radii, the field strength decreases significantly more slowly than near the ion, and the growth is mainly determined by intermolecular forces described by the Lennard-Jones potential.

LBE SIMULATION OF SATURATED VAPOR CONDENSATION UNDER THE INFLUENCE OF ELECTRIC FIELDS

The relatively new lattice Boltzmann equations (LBE) method is a discrete continuum model [14]. Presently, the LBE method can easily be competitive with common methods of numerical hydrodynamics, and it is rather preferable in certain regions (multiphase and multicomponent flows). In the simulation of phase transitions, the LBE is used as a level set method for phase interfaces [15–17].

The 3D computer simulation of a two-component air–supersaturated vapor medium was carried out accounting for condensation, evaporation, and coalescence of droplets in the electric fields. As a model system, a medium was considered consisting of inert gas and saturated vapors capable of being condensed into liquid. For vapor and liquid, a model van der Waals equation of state was used. The inert gas was described by the ideal gas law.

For nonpolar dielectrics, the Clausius–Mossotti formula was used as the dependence of the dielectric constant ε on the volume charge density ρ :

$$\varepsilon = 1 + 3\alpha\rho/(1 - \alpha\rho).$$

Here α is the polarizability.

The dynamics of gaseous and liquid phases was LBE simulated, and the potential of the electric field with taking into account the varying dielectric constant was calculated by the Poisson equation

$$\nabla(\varepsilon\nabla\varphi) = -4\pi q,$$

where the electric field vector $\mathbf{E} = -\nabla\varphi$, φ is the electrostatic field potential, and q is the electric charge.

There appear forces in the electric field acting on the dielectric:

$$\mathbf{F} = q\mathbf{E} - \frac{E^2}{8\pi}\nabla\varepsilon + \frac{1}{8\pi}\nabla\left[E^2\rho\left(\frac{\partial\varepsilon}{\partial\rho}\right)_T\right].$$

Here E is the electric field amplitude. The derivative is calculated at the constant temperature T .

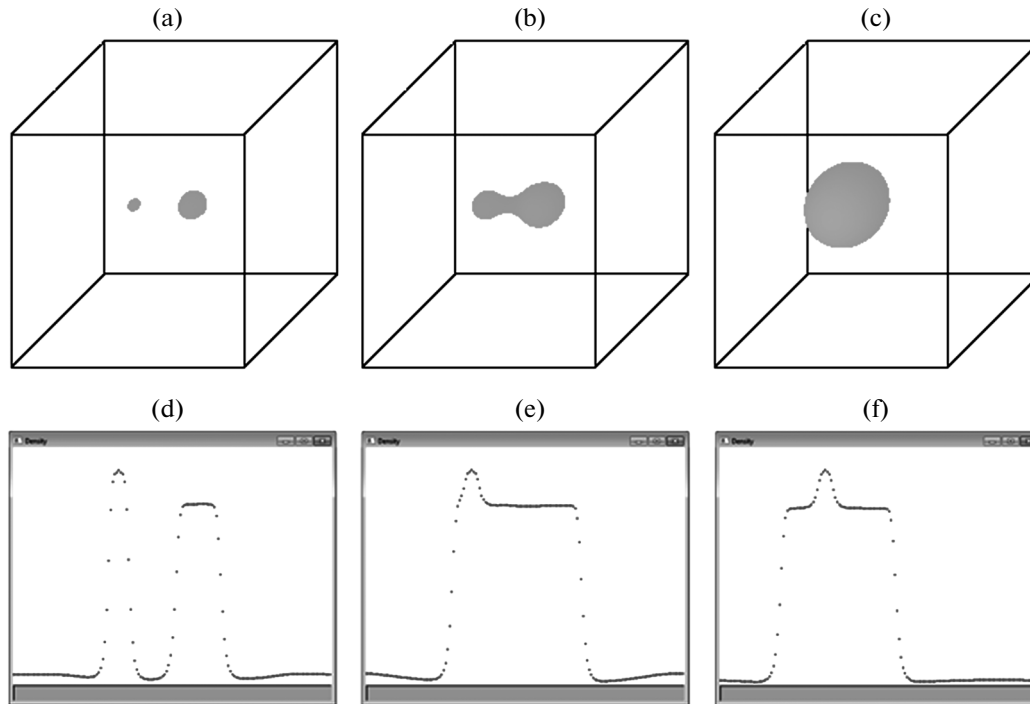


Fig. 10. (a–c) Vapor condensation on an ion and coalescence of charged and non-charged drops; (d–f) density along the symmetry axis x . $t = 250$ (a and d), 1000 (b and e), 3500 (c and f) time steps; $160 \times 160 \times 160$ grid.

The vapor condensation was simulated in the presence of point charges (ions). The drawing of the dielectric into the strong field proceeds and results in the formation of droplets close to ions serving as the condensation nuclei. Figure 10 shows the positions of droplets and medium density along the x axis.

In order to take into account thermal processes during condensation of droplets, a version of the LBE method was developed. It takes into account heat transfer [15], in which the level set method is used for calculation of liquid–vapor interfaces. It does not require the separation of phase interfaces and imposing boundary conditions on them. The algorithm takes into account the thermal conductivity, work of pressure forces, and latent heat of a phase transition.

Figure 11 shows the behavior of two droplets in a saturated vapor. The temperature of the smaller droplet is lower due to evaporation, and the larger droplet is heated due to the condensation. It was found that small droplets are cooled and the process of their evaporation in near-saturated vapor slows down when considering the heat of a phase transition.

CONCLUSIONS

The improvement of the instrumentation complex, the chamber volume of which multiply exceeds the earlier ones, allowed us to improve the reproducibility of experimental data and to widen the range of particles under analysis from nanoparticles to droplets.

The dependence of the intensity of droplet-scattered radiation on the ionizing radiation effect is found. Processes of aerosol formation, clearly seen in a water–air mixture, are shown to be significantly weaker in mixtures of water with molecular gases CO_2 and N_2 . The nucleation was observed as the result of gas medium ionization and relatively smooth relaxation of the condensation nuclei with time. We plan to actualize the step regulation of the electron beam energy and determine the influence of additions of easily ionized molecular admixtures on the condensation of water vapors in air and gas mixtures.

Generation of a micro-droplet from dense gas molecules on an ion are calculated at different values of the vapor density. In accordance with the calculations, the liquid phase nucleation on ions proceeds faster than on fluctuations of the vapor density. In an inhomogeneous field, dipole molecules settle on an ion. The influence of the electric field on the dynamics of micro-droplet generation is significant as long as the dipole layer thickness is equal to 2–3 diameters of molecules. At greater droplet radii, the field strength decreases significantly more slowly than close to the ion, and the droplet growth is determined in greater degree by intermolecular forces described by the Lennard-Jones potential.

From the macroscopic point of view, the dielectric is drawn into the strong field region, which leads to clusterization of water molecules near ions, which serve as nuclei of the further condensation. Just this

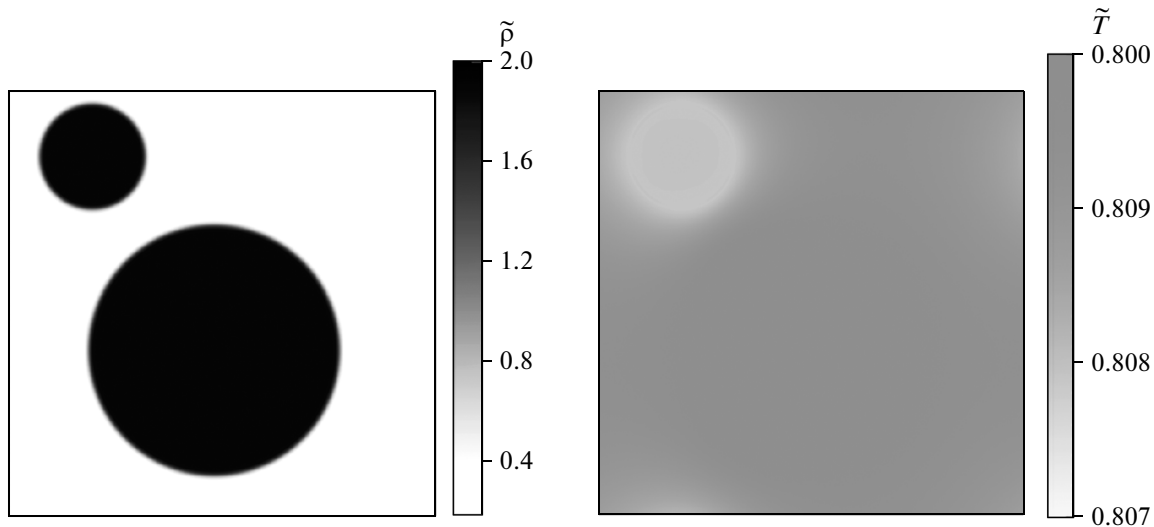


Fig. 11. (a) Density and (b) temperature distributions during a late stage of droplet coalescence (dimensionless temperature $\tilde{T}_0 = 0.8$; dimensionless density $\tilde{\rho}_0 = 0.8$; $t = 1750000$ time steps); 500×500 grid.

process is observed in mesoscopic LBE calculations. Then the generated charged droplet attracts the neighboring noncharged ones, which results in their coalescence. In addition, large droplets grow due to condensation of saturated vapor. These effects lead to the growth of the mean size of the droplets.

ACKNOWLEDGMENTS

The authors would like to thank academician G. F. Krymskii for his attention to this work and for his support.

This work was conducted with the support of the Siberian Branch of the Russian Academy of Sciences (Integration Project of Interdisciplinary Fundamental Research no. 79).

REFERENCES

1. E. P. Ney, "Cosmic radiation and the weather," *Nature (Gr. Brit.)* **183**, 451–452 (1959).
2. N. Marsh and H. Svensmark, "Cosmic rays, clouds and climate," *Space Sci. Rev.* **94** (1–2), 215–230 (2000).
3. M. Andreas, B. Enghoff, and H. Svensmark, "The role of atmospheric ions in aerosol nucleation: A review," *Atmos. Chem. Phys.* **8** (16), 4911–4923 (2008).
4. G. F. Krymskii, "Cosmic rays and the weather," *Nauka Tekh. Yakutii*, No. 1 (8), 3–6 (2005).
5. D. J. Wilson, *Wilson Chamber* (Izd. Inostr. Liter., Moscow, 1954) [in Russian].
6. A. E. Nielsen, *Kinetics of Precipitation* (Pergamon, Oxford, 1964).
7. G. F. Krymskii, V. V. Kolosov, A. P. Rostov, and I. S. Tyryshkin, "Experimental setup for investigating the water vapor nucleation in an artificial atmosphere," *Opt. Atmos. Okeana* **23** (9), 820–825 (2010).
8. G. F. Krymskii, V. V. Kolosov, and I. S. Tyryshkin, "Vapor condensation under the ionizing effect," *Opt. Atmos. Okeana* **23** (9), 826–829 (2010).
9. Yu. N. Ponomarev, A. V. Klimkin, A. S. Kozlov, V. V. Kolosov, G. F. Krymskii, A. N. Kuryak, S. B. Malyshkin, and A. K. Petrov, "Study of condensation of supersaturate water vapor under ionization of the atmosphere and accompanying characteristic IR radiation," *Solnechno-Zemnaya Fiz.*, No. 21, 58–61 (2012).
10. V. F. Tarasenko, S. I. Yakovlenko, V. M. Orlovskii, A. N. Tkachev, and S. A. Shunailov, "Production of powerful electron beams in dense gases," *J. Experim. Theor. Phys. Lett.* **77** (11), 611–615 (2003).
11. N. N. Das Gupta and S. K. Ghosh, "Wilson chamber and its application to physics," *Rev. Mod. Phys.* **18** (2), 225–365 (1946).
12. A. G. Amelin, *Theoretical Foundations of Fogging during Vapor Condensation* (Khimiya, Moscow, 1972) [in Russian].
13. J. Kolafa, "Time-reversible always stable predictor-corrector method for molecular dynamics of polarizable molecules," *J. Comput. Chem.* **25** (3), 335–342 (2003).
14. S. Chen and G. D. Doolen, "Lattice Boltzmann method for fluid flow," *Annu. Rev. Fluid Mech.* **30**, 329–364 (1998).
15. X. Shan and H. Chen, "Lattice Boltzmann model for simulating flows with multiple phases and components," *Phys. Rev. E* **47** (3), 1815–1819 (1993).
16. A. L. Kupershtokh, D. A. Medvedev, and D. I. Karpov, "On equations of state in a lattice Boltzmann method," *Comput. Math. Appl.* **58** (5), 965–974 (2009).
17. A. L. Kupershtokh, D. A. Medvedev, and I. I. Griбанov, "Modeling of thermal flows in a medium with phase transitions using the lattice Boltzmann method," *Vychislitel'nye Metody Programirovanie* **15** (2), 317–328 (2014).

Translated by S. Ponomareva